Nanoscale

Dynamic Article Links

Cite this: *Nanoscale*, 2012, **4**, 3901

www.rsc.org/nanoscale

PAPER

High-sensitivity *in vivo* imaging for tumors using a spectral up-conversion nanoparticle $NaYF_4$: Yb^{3+}, Er^{3+} in cooperation with a microtubulin inhibitor†

Yanchun Wei, Qun Chen, Baoyan Wu, Aiguo Zhou and Da Xing*

Received 4th April 2012, Accepted 28th April 2012
DOI: 10.1039/c2nr30804e

Fluorescein has been used for *in vivo* imaging to identify tumors. However, this technique presents several limitations, mainly due to its limited targeting efficiency, tissue autofluorescence and poor light penetration in tissue. In the present study, an alternative fluorescence imaging technique to localize tumors has been developed by using up-conversion nanoparticles (UCNs) and enhanced targeting approaches. A folic acid molecule is conjoined with UCNs ($NaYF_4$: Yb^{3+}, Er^{3+}) to improve the tumor-specificity; the UCN is also loaded with the microtubule inhibitor CA4P, to further improve the local delivery of particles in the tumor. The proposed imaging technique combines several well-established individual concepts into one novel integrated procedure and significantly improves its tumor-imaging capability: the near-infrared excitation for UCNs minimizes tissue autofluorescence and allows imaging into deeper tissue; the improvement in the signal to noise ratio (SNR) is at least a magnitude better than that of a conventional fluorescence imaging technique, and the modification of UCNs with folic acid significantly improves the tumor targeting efficiency by utilizing its affinity for the folic acid receptor that is often over expressed in tumors. The loading of CA4P further helps UCNs to cross blood vessel walls to reach tumor cells by depolymerizing the microtubules of endothelial cells. The integrated nanoparticle possesses the near-infrared-identical optical properties of UCNs alone, thus achieving a highly effective fluorescence imaging probe. The results demonstrated that the proposed method provides an excellent alternative for tumor localization and a potential traceable vehicle for highly efficient drug delivery.

Introduction

The diagnosis and localization of tumors are critical for their treatment.[1,2] An early and precise identification of a tumor may significantly improve its treatment outcome. At the same time, damage to the adjacent normal tissue must be minimised.

As one of the traditional imaging methods, fluorescence imaging has been used for tumor diagnosis and monitoring.[3,4] Up-conversion nanoparticles (UCNs) produced from rare-earth ions are a novel candidate material for an alternative approach to enhanced fluorescence imaging.[5–7] The particles are phosphors that absorb infrared-light photons and subsequently emit visible-light photons.[8,9] The up-conversion fluorescence of UCNs is a process where continuous-wave (CW) low-energy light in the near-infrared region (typically 980 nm) is converted to higher energy visible light through sequential absorption of multiple photons or energy transfer.[10,11] In addition, as a rare-earth nanoparticle, a UCN has advantages towards drug loading and carrying and its use as a drug vehicle has been reported.[12–15]

A preferential affinity of UCNs to tumor cells is essential for potential localization and diagnostic purposes. Nanoparticles can be modified with specific molecules on their surface to achieve a high affinity to the corresponding target cells. This technique is based on an interaction between ligand and receptor, and has been widely studied and applied in various biological and medical applications.[16] In this study, we used the ligand molecule folic acid attached on the UCN surface to help facilitate the specific uptake of UCNs by tumor cells.[17] Folic acid (also known as vitamin B9 or folacin) is essential to numerous bodily functions ranging from nucleotide biosynthesis to the remethylation of homocysteine. For many tumor cells, folic acid is greatly needed for malign hyperplasia and this leads to a significant increase in the presence of folate receptors compared to that in normal tissues.[18] Tumor cells with over expressed folate receptors may increase the efficiency of UCN targeting.

To serve as an imaging probe, UCNs must cross the vascular wall to reach tumor cells. The cells can then endocytose them based on the interaction between ligands and receptors. Commonly, few macromolecular drugs and nanoparticles can pass through blood vessels into normal tissue, but this is possible

MOE Key Laboratory of Laser Life Science & Institute of Laser Life Science, College of Biophotonics, South China Normal University, Guangzhou 510631, China. E-mail: xingda@scnu.edu.cn; Fax: +86-20-85216052; Tel: +86-20-85210089

† Electronic supplementary information (ESI) available. See DOI: 10.1039/c2nr30804e

in tumors due to anatomical and pathophysiological alteration.[19] The process of angiogenesis is essential for tumors to develop and grow beyond a volume of 2–3 mm. The stimulation of new blood vessel formation in response to continuous proangiogenic factor signalling by tumor cells results in a state of angiogenesis not normally present in adult tissues. The blood vessels resulting from this process are typically aberrant in structure and function, and characterized as leaky, tortuous, and lacking normal pericyte interaction. Although this phenomenon of enhanced permeability and retention (known as the EPR effect) benefits the drug and nanoparticle delivery, the permeation efficiency is still insufficient for biomedical application, thus many agents and methods have been studied to improve the EPR effect.[20]

The EPR effect can be augmented by drugs. Cell microtubulin inhibitors have been reported to enhance vascular permeability.[21] Microtubulin is one of the important cytoskeletal filaments for providing a cell with structure and shape. The active species of tubulin-binding agents bind reversibly to tubulin subunits and, in proliferating endothelial cells, lead to the depolymerization of the microtubule and ultimately result in its detachment. These agents show promise as tumor vascular targeting agents.

Combretastatin-A4-phosphate (CA4P) is a potent inhibitor to the inducement of microtubule depolymerization, causing cell morphological change and cell division to stop, and even inducing cell apoptosis. More importantly, it can specifically act on tumor vascular cells[22] and the tumor vascular permeability can be effectively increased by employing this agent.[23] In our study CA4P was carried by UCNs to promote more particles to cross through the vascular wall, achieving high efficiency up-conversion fluorescence localization. The hypothetical principle is shown as Scheme 1A.

Materials and methods

Folic acid modification and CA4P loading

$NaYF_4$: 10 mol% Yb^{3+}, 1 mol% Er^{3+} nanocrystals coated with PEI (polyethylenimine) was synthesized by Prof. Xianggui Kong's research group. To analyze the amine moieties on the UCNs, 1 mg of UCNs was weighed. Amine quantification was performed using the Element Analyzer (EA2400II, PerkinElmer, USA) by detection of the element nitrogen. The shape and size were also detected with a transmission electron microscope (TEM). Samples of UCNs were prepared by placing a drop of a dilute aqueous dispersion on the surface of a copper grid. The sizes and morphologies of the UCNs were determined at 200 kV using a JEOL JEM-2010F high-resolution transmission electron microscope (HR-TEM).

The nanoparticles (10 mg) were resuspended in 5 ml deionized water. Folic acid was prepared to modify the nanoparticles. The more reactive γ-carboxylic acid of folic acid (2.25 mg, 5×10^{-6} mol) was activated with EDC/NHS (2×10^{-4} mol) in DMSO (10 ml) solution.[24] 30 min later, the activated folate solution was slowly added to the PEI-coated UCN solution and then stirred at room temperature for 4 h. The reaction product was purified by centrifugation at 10 000 rpm (10 612 × *g*) for 10 min and suspended in 5 ml of DMSO (repeated three times for purification). Finally, the folic acid conjugated UCN (UCN-FA) was dissolved in 5 ml of PBS.[25]

CA4P (2 mM) was prepared as a stock solution and stored at 4 °C. UCN-FA (4 mg) was added to the CA4P solution (1 ml) and stirred at room temperature for 24 h. The UCN-FA-loaded CA4P (UCN-FA-CA4P) was then isolated by centrifugation and decantation. To determine the drug loading rate, several concentrations of CA4P (5, 15, 25, 35, 45, 55 μM) were prepared and their absorptions in a quartz cell at 295 nm were detected by a UV-vis spectrometer (Lamda35, Perkin Elmer, Shelton, USA) to build a standard curve. The supernatant was diluted 20 times with ultra-pure water and the CA4P concentration was detected by the spectrometer. Finally the sample was washed three times with pure water and redispersed in 2 ml PBS (pH: 7.4) for use. (The surface modification and drug loading are represented by Scheme 1B.)

Desiccant PEI-coated UCNs and UCN-FA-CA4P (1 mg) were prepared. Fourier transform infrared (FT-IR) spectra were recorded with KBr pellets on a Bio-Rad FTS 6000 spectrometer (Bio-Rad Company, Hercules, California, USA) at room temperature. The nanoprobe UCN-FA-CA4P was diluted with deionized water and the hydrodynamic size was detected by a particle size instrument (Zetasizer nano-ZS90, Malvern Instruments Ltd., Malvern, UK).

Up-conversion fluorescence detection in solution

PEI-coated UCN, UCN-FA and UCN-FA-CA4P (500 μl, 1 mg ml^{-1}) were each put into quartz Cuvettes. By excitation with a laser (980 nm, 150 mW cm^{-2}, semiconductor laser, NL-FBA-30-980, nLight Photonics Corporation, Vancouver, WA, USA), emission spectra from 500–700 nm were detected with a fluorescence spectrometer (LS-55, Perkin Elmer, Shelton, USA).

By dissolving the UCNs and UCN-FA (0.5 mg ml^{-1}) in different media (water, PBS, DMEM and 5 μM CA4P) in glass dishes, the total intensity of the fluorescence excited at different laser fluence rates (0.16, 0.32, 0.64, 1.28 and 2.56 mW cm^{-2}) was measured with an ICCD instrument (ICCD-576-s/1–35 °C; Princeton Instruments, USA). To evaluate photobleaching, both UCN-FA and UCN-FA-CA4P (1 ml solution) were continuously exposed to a 980 nm laser at 800 mW cm^{-2} for 12 h and the fluorescence intensity was measured every 2 h.

Up-conversion fluorescence *ex vivo* and UCN-FA targeting *in vitro*

Chicken breast tissue was frozen at −20 °C and sliced to 1 mm thickness with a freezing microtome (CM1850, Leica, Germany). An indent ($\Phi = 1$ mm) drilled in a thick plastic board was filled with UCNs (2 mg ml^{-1}, 1 μl) or fluorescein sodium (50 μM, 1 μl). The indent was covered with 2 mm chicken tissue. The sample was irradiated with different laser fluence rates (UCN: 20–300 mW cm^{-2}, 980 nm; fluorescein sodium: 20–70 mW cm^{-2}, 488 nm). Images were recorded and SNRs of the UCNs and fluorescein sodium were calculated accordingly.

The slice of chicken tissue (0.3 mm or 1 mm) was used in turn to cover the indent. With laser excitation (UCN: 500 mW cm^{-2}, 980 nm; fluorescein sodium: 30 mW cm^{-2}, 488 nm), the SNRs of the images were analyzed.

Lung adenocarcinoma ASTCa-1 cells that are known to have overexpressed the folic acid receptor[26] (purchased from Fourth

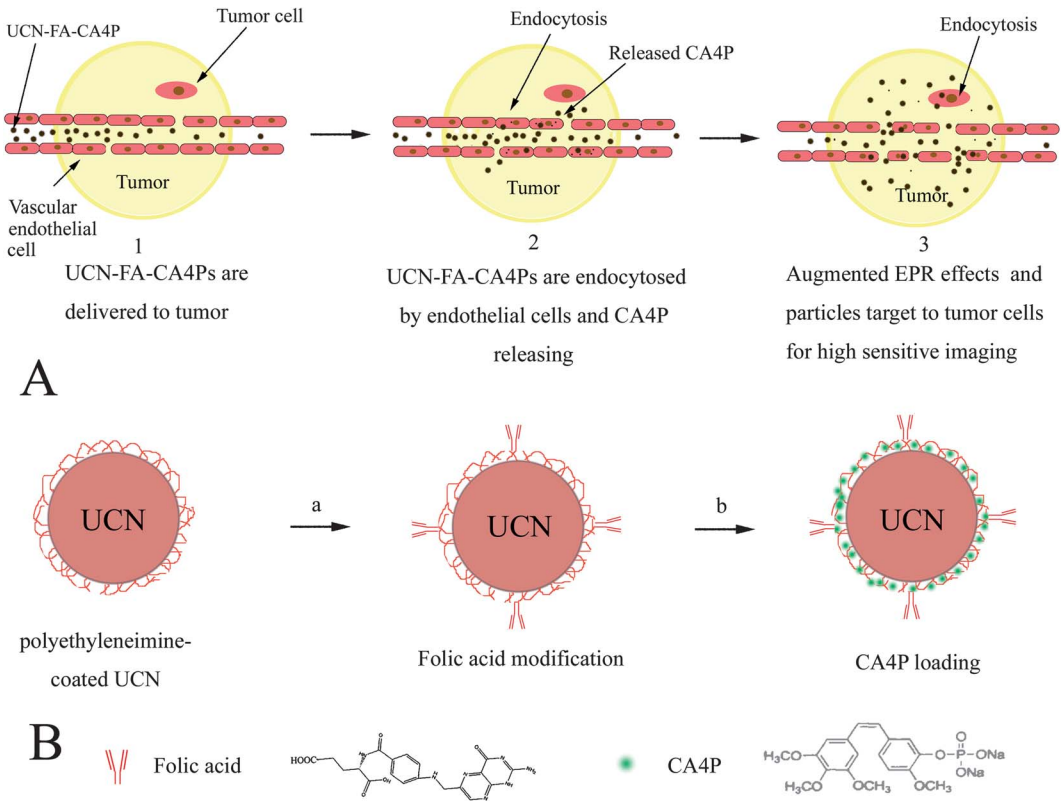

Scheme 1 (A) Enhancement of the targeting efficiency of UCNs by cooperation with CA4P. (B) Schematic representation of UCN-targeted modification and drug loading.

Military Medical University Experimental Centre) were cultured in DMEM with 10% FCS at 37 °C in four glass dishes (1×10^5 cells per dish). Three dishes were incubated with UCNs, UCN-FA and UCN-FA-CA4P, respectively, (1 mg ml^{-1}, 100 μl) for 2 h; one dish was pre-incubated with folic acid (1 mM) for 1 h before being incubated with UCN-FA. All the cells were washed three times with PBS before being imaged with a fluorescence microscope (ECLIPSE 80i, Nikon, Japan) with a 400 mW cm^{-2} laser excitation.

Cell microtubulin staining and tumor blood perfusion

Human umbilical vein endothelial cells (HUVEC, purchased from Fourth Military Medical University Experimental Centre) were cultured in DMEM, 10% FCS at 37 °C in three dishes (0.5×10^5 cells per dish). After attachment culture for 24 h, one dish of untreated cells was used as a control while the cells in the other dishes were incubated with 2.5 μM of CA4P and 5 μM of UCN-FA-CA4P (0.1 mg ml^{-1}) for 24 h, respectively. All the dishes were subjected to immunol staining with Tubulin-Tracker Red (Beyotime Institute of Biotechnology, Shanghai, China). Tubulin-Tracker Red, a red immunol fluorescence probe for cell tubulin staining, is an anti α-tubulin mouse monoclonal antibody marked with Alexa Fluor 555. The maximum excitation and emission wavelengths are 555 nm and 565 nm, respectively. All the staining steps were carried out according to the manufacturer's information. The stained cells were monitored by a laser confocal microscope (LSM 510 Meta, Carl Zeiss, Jena, Germany) for potential morphological change.

To measure the blood perfusion of the tumor, three mice injected with CA4P (i.p., 20 mg kg^{-1}) and three mice injected with UCN-FA-CA4P (i.v., 1 mg ml^{-1}, 200 μl) were anaesthetized and positioned on a platform at 0, 12, 24, 36 and 48 h. The probe (Probe 418-1, Perimed, Stockholm, Sweden) of the laser Doppler flow meter (PeriFlux System 5000, Perimed) was inserted under the tumor skin, with the guidance of a dermal needle mounted on a 3-D micromanipulator stage. The blood perfusion was measured for 60 seconds each time.

Up-conversion fluorescence imaging *in vivo*

Balc/a nude mice (5 weeks old) were obtained from the Animal Experimentation Center at Sun Yat-sen University (Guangzhou, China). Animal procedures were in agreement with the guidelines of the Institutional Animal Care and Use Committee. The cells (1×10^7 cells per ml, 100 μl) were inoculated subcutaneously into the back of the nude mice. Once the volume approached 300 mm^3, the mice were divided into five groups (4 per group) and anaesthetized with pentobarbital sodium (i.p., 60 mg kg^{-1}). The mice, except the control group, were injected with different nanoparticles (i.v., 1 mg ml^{-1}, 200 μl): PEI-coated UCNs, UCN-FA, UCN-FA and CA4P (20 mg kg^{-1}, simultaneously injected by i.p.), and UCN-FA-CA4P. The mice were irradiated with a laser (980 nm, 300 mW cm^{-2}) and imaged with a pre-cold ICCD camera at 0, 24 and 48 h after injection.

Nanoparticle plasma-mass spectrometry analysis

Nanoparticle uptake in tumors was evaluated with inductively coupled plasma mass spectrometry (ICP-MS) analysis (Agilent 7500a, Agilent, America). After imaging, the mice were sacrificed. The tumors were homogenized in deionized water (5 ml) and HNO_3 (100 μl). The product was further diluted with deionized water to 1 : 25. The yttrium (Y) content in the samples was then determined using ICP-MS as a means of determining the nanoparticle concentration.[11] The data are presented from the average of three experimental animals.

Results

Fig. 1A shows the emission spectra of the PEI-coated UCNs (α-$NaYF_4$:Yb/Er), the folate molecule modified UCNs and CA4P-loaded UCN-FA. The results indicate that the fluorescence spectra have peaks at 521, 540 and 654 nm. The emission spectrum remained stable regardless of the modification. The fluorescence image of UCN-FA in an Eppendorf tube is included in the Figure. The TEM image and statistical distribution chart show that the UCN sample is dispersed with an average diameter of 50 nm (Fig. 1B). A validated FT-IR examination shows three peaks at 3420, 1633 and 1444 cm^{-1}, which are assigned to the vibrations of the NH_2 group of PEI (Fig. 1C). By analyzing the nitrogen content with an Element Analyzer, the amine content of the UCNs was found to be about 7.5×10^{-3} mol g^{-1}. In Fig. 1D, the existence of the peaks at 1355, 1328 and 1236 cm^{-1} (C–H bending vibration of substituted aromatic ring), 1124 and 1058 cm^{-1} (P–O and C–O–C stretching vibration), 951 and 900 cm^{-1} (C–H bending vibration of prosubstituted aromatic ring) prove that CA4P has been successfully loaded onto UCN-FA by physical absorption. The hydrodynamic size of UCN-FA-CA4P was measured by dynamic light scattering. The average size is 145 nm and its distribution is shown in Fig. 1E. The CA4P concentration in the supernate after centrifugation was determined by the acquired standard curve. The loading rate can be calculated by the equation drug loading rate = (original drug concentration − supernatant drug concentration)/original drug concentration × 100%. The calculation shows a 71% CA4P loading rate. Fig. S1† further shows the CA4P releasing rate from the integrative functional nanoparticle. The rate reached a stable level after 10 hours and more than 55% CA4P was retained.

The up-conversion fluorescence intensity is influenced by the UCN-FA concentration and increases linearly with the square of the irradiation fluence rate, which is consistent with that of a two-photon absorption (Fig. S2†). As the fluorescence properties of the fluorophore are often affected by their chemical/physiological environment, the UCNs were dissolved in several aqueous solutions, including deionized water, pH 7.4 PBS, a DMEM solution and a CA4P solution (Fig. 2A). The results indicate that the fluorescence intensity of UCN-FA is insensitive to its potential environment for *in vivo* applications. Probe photobleaching often poses a significant drawback for fluorescence imaging: the UCNs exhibited a stable luminescence even at a high fluence rate of irradiation (Fig. 2B).

As the three types of up-conversion nanoparticles have similar luminescence characteristics, only UCN-FA was used for the fluorescence signal ratio detection. Fig. 3 evaluates the SNR of UCN-FA at different laser fluence rates (Fig. 3A) and tissue

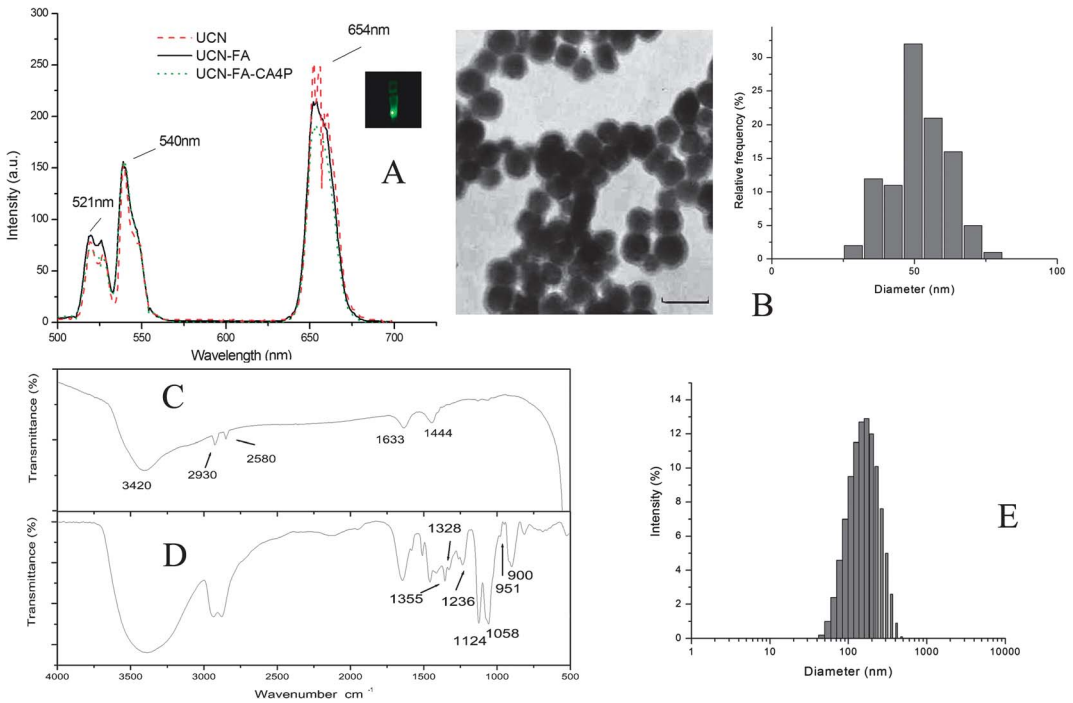

Fig. 1 The optical properties of nanoparticles. (A) Emission spectra of the PEI-coated UCNs, UCN-FA and UCN-FA-CA4P from 500–700 nm. The inset shows (A) the fluorescence image of UCN-FA in an Eppendorf tube, (B) a transmission electron microscopy (TEM) image and the particle size distribution – the scale bar is 100 nm. (C and D) Fourier transform infrared (FT-IR) spectra of the PEI-coated UCNs (C) and UCN-FA-CA4P (D). (E) The hydrodynamic size distribution of UCN-FA-CA4P, the average diameter is 145 nm.

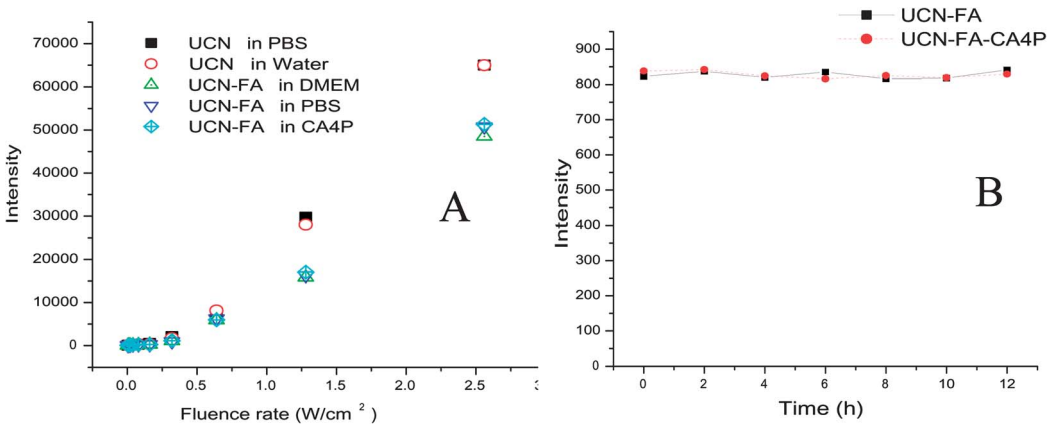

Fig. 2 Fluorescence stability of particles. (A) The intensity of UCN-FA dissolved in different aqueous solutions. (B) The anti-photobleaching capability of UCN-FA. UCN-FA was irradiated for 12 h continually with a laser (980 nm, 800 mW cm^{-2}).

depths (Fig. 3B) by comparison with fluorescein sodium. The results show that the SNR of UCN-FA shows exponential growth but the fluorescein sodium increases logarithmically with the increased laser fluence rate. In addition, the SNR of fluorescein sodium decreases six times faster than that of UCN-FA when the tissue thickness increases. The SNR of UCN-FA at 3 mm tissue depth is 12 times higher than that of fluorescein sodium. The comparison of the fluorescence intensities between UCN-FA and quantum dots in different tissue depths also shows the same advantage (Fig. S3†).

The targeting specificity of UCN-FA and UCN-FA-CA4P to tumor cells was studied *in vitro*, to prove the binding capability of the ligands and receptors. The cell fluorescence intensities in the four groups were compared (Fig. 4) and the results indicate that the up-conversion fluorescence intensity of both UCN-FA and UCN-FA-CA4P are stronger than the other cell groups, including the UCN-only group and the pre-incubated folic acid group.

After being incubated with CA4P and UCN-FA-CA4P for 24 h, the cell cytoskeleton was disrupted. Fig. 5A shows that the microtubule system was intact in the control group, presenting a filamentous network. However, in the CA4P and UCN-FA-CA4P groups, the cell networks were destroyed. The disintegration of the microtubule system led to cell contraction. Fig. 5B shows the profile plot along the arrows. The peaks of the control group are sharp and sparse compared to those of the other groups. In addition, Fig. S4† demonstrates the process in a multi-cell environment. Blood perfusion in the mouse tumor tissue was also detected. A minimal effect on the blood perfusion was observed after administering CA4P *in vivo* (Fig. 5C).

When CA4P was employed in the tumor-bearing mice, both fluorescence and normal white-light images of the mice were acquired at 0, 24 and 48 h. The corresponding images were overlaid to demonstrate the optical localization of the tumor. The results show that the nanoparticle-modified folic acid localized at the tumor site effectively, and the fluorescence intensity increased significantly in both the CA4P + UCN-FA and the UCN-FA-CA4P groups than those in the other two groups (Fig. 6A and B). Fig. 6C shows the result of Y ion concentrations in tumors by ICP-MS to assess the UCN content. The Y^{3+} concentration is significantly higher in the employed CA4P group. As 980 nm laser irradiation may raise the tissue temperature, thermal images were acquired to validate the thermal safety of the procedure. The results indicate that there is no hyperthermia effect during the irradiation process (Fig. S5†).

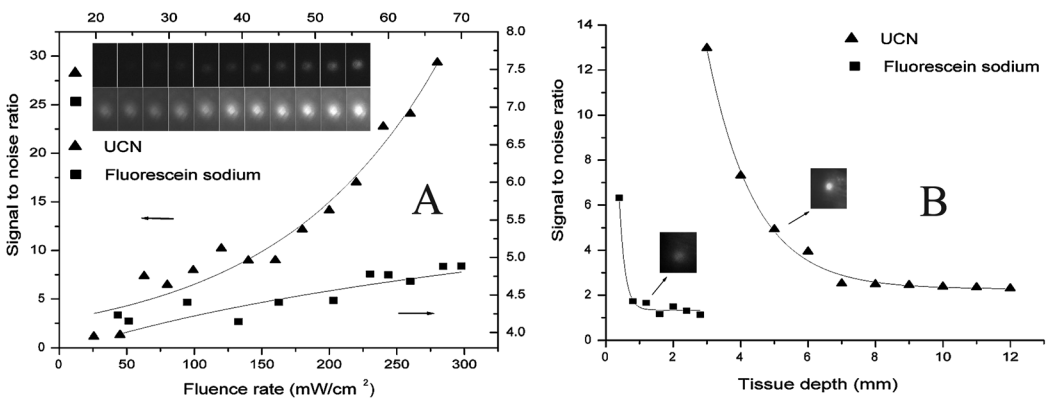

Fig. 3 Signal to noise ratio (SNR) of the UCNs and fluorescein sodium. (A) SNR of UCN and fluorescein sodium during laser excitation with different fluence rates. The data are fitted with exponential growth (UCN: $R^2 = 0.96$) and logarithmic growth (fluorescein sodium: $R^2 = 0.7$). (B) SNR of the UCNs and fluorescein sodium during laser excitation at different tissue depths. The data are fitted with exponential decay (UCN: $R^2 = 0.997$, $\tau = 1.4$; fluorescein sodium: $R^2 = 0.99$, $\tau = 0.166$).

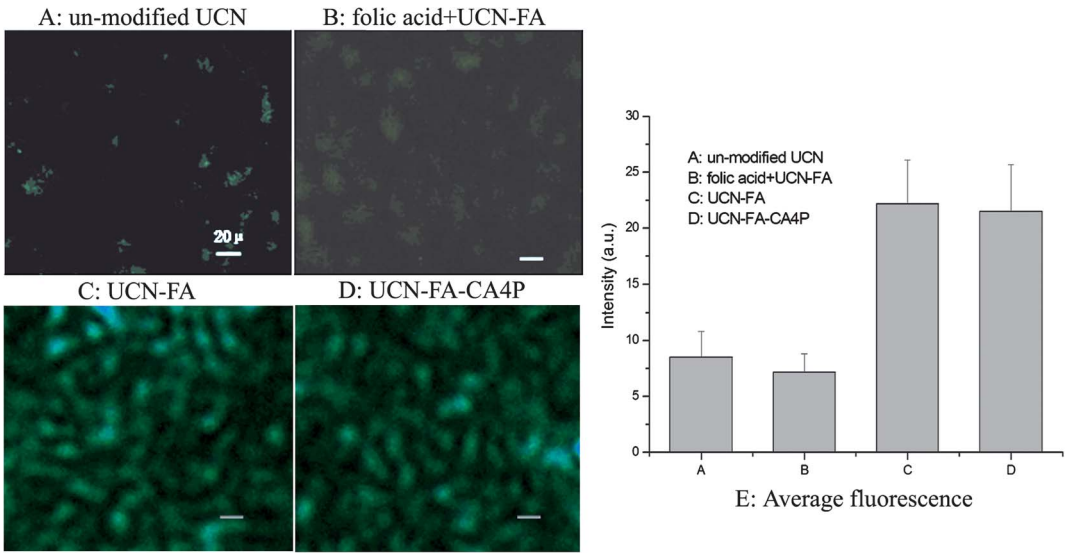

Fig. 4 Specific-targeting cellular imaging of UCN-FA. After lung adenocarcinoma cells were incubated with (A) UCN, (B) folic acid (pre) + UCN-FA, (C) UCN-FA and (D) UCN-FA-CA4P for 2 h, respectively, up-conversion fluorescence intensities were detected. The bar is 20 μm. Histogram (E) is the average fluorescence intensities of the four images, ($n = 3$).

Discussion

In conventional fluorescence imaging methods, a fluorescence probe is typically excited with light at shorter wavelengths. This is associated with several major limitations. In particular, fluorescein photobleaching and tissue autofluorescence are two serious problems, complicating the interpretation of the data and at the same time, reducing the SNR. Furthermore, photons with a short wavelength for excitation are strongly absorbed and scattered by biological tissues, which ultimately deteriorates the acquired signal.

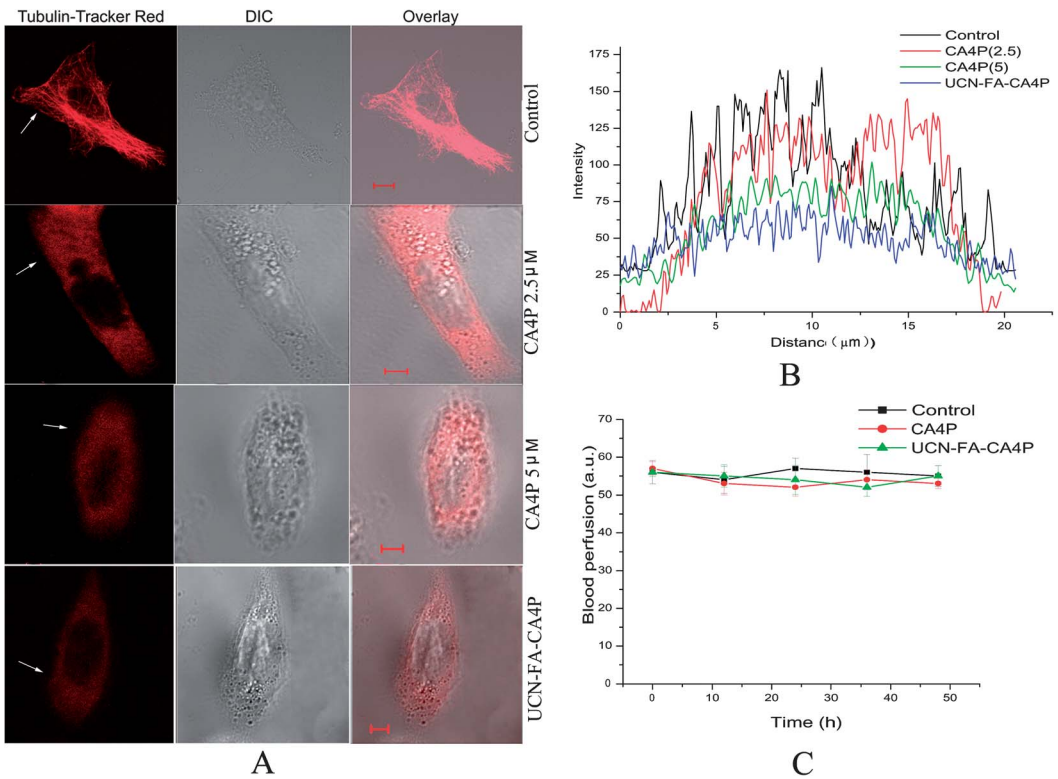

Fig. 5 Tubulin staining of cells with Tubulin-Tracker Red and tumor blood perfusion. (A) Cells in four dishes were incubated with non-CA4P, 2.5 μM CA4P, 5 μM CA4P or UCN-FA-CA4P for 24 h and then stained. The scale bar is 5 μm. (B) Profile plots of the fluorescence intensity along the arrows in (A). (C) Blood perfusion in the superficial tumor of the control group and the mice with CA4P and UCN-FA-CA4P. The data are presented as mean ± SD, $n = 3$.

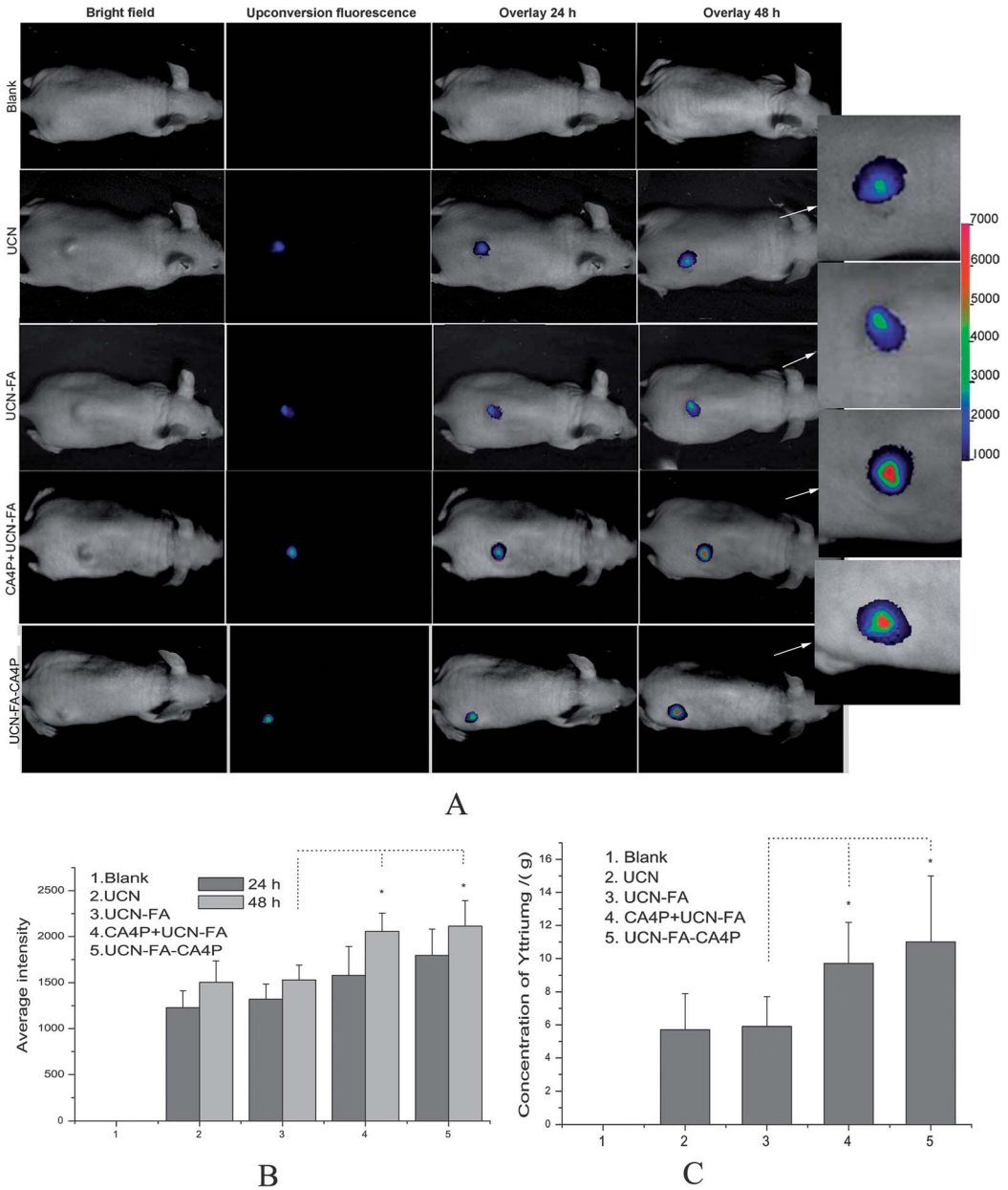

Fig. 6 *In vivo* improved targeting of up-conversion nanoparticles for tumor imaging. (A) Up-conversion fluorescence imaging of mice at 24 h and 48 h after injection with UCNs, UCN-FA, CA4P + UCN-FA and UCN-FA-CA4P, respectively. (B) The statistical result of fluorescence average intensities. (C) Y^{3+} concentration in the tumors measured by ICP-MS. The data show the particle uptake in the tumor after the different protocols were administered. The error bars are based on triplet samples. The data are presented as mean ± SD and analyzed with the student's *t*-test (*$P < 0.05$).

UCN is excited with low energy near infrared light. This leads to a significantly reduced photobleaching effect compared to that in conventional fluorescence imaging. The photon emission from the UCNs is stable in different aqueous solutions (Fig. 2A), mainly owing to its crystal structure and the inner transfer course of energy. This photo-stability will help to establish the technique for practical applications with less complex data interpretation.

To evaluate the feasibility of a novel imaging technique, the SNR is another important consideration. During UCN imaging, autofluorescence can be practically ignored due to the near-infrared excitation. The imaging, as shown in the results, can be achieved with a significantly improved SNR. It is well established that photons with longer wavelengths from 650 nm to 1300 nm have a significantly better penetrating capability compared to those at shorter wavelengths.[27] Therefore, the UCNs also have a better tissue imaging depth than other fluorophores due to their near-infrared excitation.

As an optical contrast agent, the UCN must be targeted to and retained in the intended tissue. Studies have proved that specific targeting can be achieved by molecular modification. Based on this concept, PEI-coated UCNs were modified with folic acid through an amidation reaction. It has been reported that PEI possesses a positive charge due to the terminal $-NH_2$ groups and PEI-capped nanoparticles can carry negatively charged molecules *via* the electrostatic interaction.[28] In the modification, most of the amido groups of PEI were unreacted for the limited folic

acid dose that was used. The UCN-FA thus possesses a positive charge and can load the negatively charged CA4P effectively with the same mechanism.

In addition, to understand how the properties of UCN are influenced by this modification is important. With the folic acid and CA4P loading, the particle size was increased predictably. The hydrodynamic detection result shows an increased size of the probe compared to the TEM result (Fig. 1), but the particle diameter is still within the "ideal" size requirement that allows them passage through the vascular wall.[29] The optical characteristics of the UCNs were also investigated after modification. The results show a minimal effect on the quantum efficiency and the spectral characteristics of the UCNs (Fig. 1 and 2). Similarly, the CA4P loading onto the UCNs showed a minimal effect.

The steps of the particle targeting to the tumor should include both recognition and reception by the cells. The *in vitro* result indicates that the targeting function of UCNs is achieved with the biochemical modification. The high efficiency of the cellular uptake of UCNs modified with folic acid suggests such a targeting mechanism: the folic acid receptor, a tumor associated glycosylphosphatidylinositol anchored protein, can actively internalize the bound folates and the folate-conjugated compounds *via* receptor-mediated endocytosis.[26]

Surface-modified UCNs allow specific cellular targeting and deep tissue imaging. Yet, to realize the intention *in vivo*, the particles must pass through tumor vascular wall. A porous vascular wall is prerequisite. After i.v. injection, the particles are circulated in the vascular system. Part of the particles will pass through the fenestrated blood vessel walls (named the EPR effect),[30] and subsequently is endocytosed by the tumor cells. On the other hand, concurrent with the accumulation, the intravascular and intracellular particle concentration is reduced by the metabolism. To achieve a reasonable intracellular concentration of the probe, it is important to optimize its vascular penetration efficiency.

The results of microtubule staining indicate that the microtubule system of the vascular endothelial cells was disrupted by the loss of their filamentous network during incubation with CA4P, which resulted in the morphological features changing. This increases the vascular leakage and provides a high probability of nanoparticle localization in the inter-tissue spaces of the tumor. Two routes of CA4P administration were investigated with endothelial cells; direct injection or injection as a UCN loading. The results show that CA4P loaded on UCN is an effective and reliable way for its delivery. As a validation group for the CA4P action, the direct injection also shows a similar effect but with a higher drug dose.

In experiments, CA4P was thus administered *in vivo* to enhance the nanoparticle tumor delivery efficiency by either direct injection or UCN-FA loading. Studies have reported that CA4P has antiproliferative and cytotoxic effects in both endothelial and tumor cells in culture, but mainly in endothelial cells, and is greatly dose-frequency dependent.[31–33] An over-dose may result in microvessel shut down.[34] It has been proved that a single intraperitoneal injection of CA4P at 100 mg kg^{-1} is nontoxic and elicits changes in the tumor perfusion without significantly affecting the tumor growth rates.[35] In the present experiment, a single injection and a lower dose of CA4P (20 mg kg^{-1}) was administered and the blood flow was investigated for potential side effects. The results (Fig. 5C) demonstrate that the CA4P dosage used for this application had little effect. It can thus be concluded that the dosage of CA4P administered in the experiment would have a minimal influence on cancer cell growth and not affect the tumor development.

With near-infrared excitation, real-time fluorescence images were captured to demonstrate its effect on the localization process (Fig. 6A). The results show that the fluorescence intensity at 48 h was stronger than that at 24 h, indicating the particle accumulation in the tumor is a time-dependent process. Comparing the UCN and UCN-FA groups, the fluorescence intensities are similar. This result indicates that the particle modification alone did not significantly improve the fluorescence imaging. However, with the CA4P administered to the mice, the up-conversion fluorescence was enhanced greatly, suggesting that the blood vessel permeability was increased and more UCN-FA was accumulated in the tumor. This result is validated by direct detection of the particle concentration with ICP-MS. In the UCN-FA-CA4P group, the significantly increased fluorescence means that the CA4P loaded onto the particles had acted upon the endothelial cells. During the particle targeting course, UCN-FA-CA4P ingested by receptor-mediated endocytosis by endothelial cells is likely to be the main route for drug delivery. By comparison of direct injection and UCN-loading of CA4P, the later is clearly more effective and less complicated in practice.

Conclusions

The up-conversion fluorescence excited by near-infrared light can significantly improve imaging sensitivity and quality from deeper tissue, with minimal interference from autofluorescence. By modifying UCNs with folic acid to improve tumor targeting and administering CA4P to improve tumor delivery of the probe, the quality of the fluorescence imaging can be significantly improved further. With the integration of up-conversion nanoparticles, folic acid and Combretastatin-A4-phosphate, a highly efficient targeting nanoparticle is constructed. A novel imaging technique with a high SNR is thus established. This method is likely to provide a highly sensitive fluorescence imaging technique for tumor diagnosis and localization, and a highly efficient drug delivery method with fluorescence monitoring.

Acknowledgements

This research is supported by the National Basic Research Program of China (2011CB910402; 2010CB732602), the Program for Changjiang Scholars and Innovative Research Team in University (IRT0829), and the National Natural Science Foundation of China (81101741). The authors thank Dr Xianggui Kong, Key Laboratory of Excited State Process, Changchun Institute of Optics, Fine Mechanics and Physics, Chinese Academy of Sciences, Changchun, China for providing the up-conversion nanoparticles. No conflict of interest was reported by the authors of this article.

Notes and references

1 J. A. Barreto, W. O'Malley, M. Kubeil, B. Graham, H. Stephan and L. Spiccia, *Adv. Mater.*, 2011, **23**, H18–H40.

2 M. Oostendorp, K. Douma, T. M. Hackeng, A. Dirksen, M. J. Post, M. A. van Zandvoort and W. H. Backes, *Cancer Res.*, 2008, **68**, 7676–7683.
3 C. Balas, *Meas. Sci. Technol.*, 2009, **20**, 104020.
4 Y. Saito, T. Furukawa, Y. Arano, Y. Fujibayashi and T. Saga, *Nucl. Med. Biol.*, 2008, **35**, 851–860.
5 G. Zhang, Y. Liu, Q. Yuan, C. Zong, J. Liu and L. Lu, *Nanoscale*, 2011, **3**, 4365–4371.
6 A. Bhirde, J. Xie, M. Swierczewska and X. Chen, *Nanoscale*, 2011, **3**, 142–153.
7 Q. Liu, Y. Sun, C. Li, J. Zhou, C. Li, T. Yang, X. Zhang, T. Yi, D. Wu and F. Li, *ACS Nano*, 2011, **5**, 3146–3157.
8 L. Cheng, K. Yang, S. Zhang, M. W. Shao, S. T. Lee and Z. Liu, *Nano Res.*, 2010, **3**, 722–732.
9 Z. L. Wang, J. Hao, H. L. Chan, G. L. Law, W. T. Wong, K. L. Wong, M. B. Murphy, T. Su, Z. H. Zhang and S. Q. Zeng, *Nanoscale*, 2011, **3**, 2175–2181.
10 L. Q. Xiong, Z. G. Chen, M. X. Yu, F. Y. Li, C. Liu and C. H. Huang, *Biomaterials*, 2009, **30**, 5592–5600.
11 D. K. Chatterjee, A. J. Rufaihah and Y. Zhang, *Biomaterials*, 2008, **29**, 937–943.
12 C. Wang, L. Cheng and Z. Liu, *Biomaterials*, 2011, **32**, 1110–1120.
13 X. F. Yu, Z. Sun, M. Li, Y. Xiang, Q. Q. Wang, F. Tang, Y. Wu, Z. Cao and W. Li, *Biomaterials*, 2010, **31**, 8724–8731.
14 C. Wang, H. Tao, L. Cheng and Z. Liu, *Biomaterials*, 2011, **32**, 6145–6154.
15 L. Cheng, K. Yang, M. Shao, S. T. Lee and Z. Liu, *J. Phys. Chem. C*, 2011, **115**, 2686–2692.
16 E. Ruoslahti, S. N. Bhatia and M. J. Sailor, *J. Cell Biol.*, 2010, **188**, 759–768.
17 Y. Teow and S. Valiyaveettil, *Nanoscale*, 2010, **2**, 2607–2613.
18 X. Zhao, H. Li and R. J. Lee, *Expert Opin. Drug Delivery*, 2008, **5**, 309–319.
19 J. Fang, H. Nakamura and H. Maeda, *Adv. Drug Delivery Rev.*, 2011, **63**, 136–151.
20 A. K. Iyer, G. Khaled, J. Fang and H. Maeda, *Drug Discovery Today*, 2006, **11**, 812–818.
21 C. Kanthou and G. M. Tozer, *Drug Discovery Today: Ther. Strategies*, 2007, **4**, 237–243.
22 T. Nielsen, R. Murata, R. J. Maxwell, H. Stodkilde-Jorgensen, L. Ostergaard, C. D. Ley, P. E. Kristjansen and M. R. Horsman, *Acta Oncol.*, 2010, **49**, 906–913.
23 C. C. Reyes-Aldasoro, I. Wilson, V. E. Prise, P. R. Barber, M. Ameer-Beg, B. Vojnovic, V. J. Cunningham and G. M. Tozer, *Microcirculation*, 2008, **15**, 65–79.
24 S. L. Kim, H. J. Jeong, E. M. Kim, C. M. Lee, T. H. Kwon and M. H. Sohn, *J. Korean Med. Sci.*, 2007, **22**, 405–411.
25 S. Jiang and Y. Zhang, *4th Kuala Lumpur International Conference on Biomedical Engineering 2008*, vol. 1 and 2, 2008, 21, pp. 330–332.
26 P. S. Low, W. A. Henne and D. D. Doorneweerd, *Acc. Chem. Res.*, 2008, **41**, 120–129.
27 B. C. Michael, S. Patterson and B. C. Wilson, *Appl. Opt.*, 1989, **28**, 2331–2336.
28 W. J. Song, J. Z. Du, T. M. Sun, P. Z. Zhang and J. Wang, *Small*, 2010, **6**, 239–246.
29 M. Gaumet, A. Vargas, R. Gurny and F. Delie, *Eur. J. Pharm. Biopharm.*, 2008, **69**, 1–9.
30 J. H. Park, G. von Maltzahn, M. J. Xu, V. Fogal, V. R. Kotamraju, E. Ruoslahti, S. N. Bhatia and M. J. Sailor, *Proc. Natl. Acad. Sci. U. S. A.*, 2009, **107**, 981–986.
31 G. G. Dark, S. A. Hill, V. E. Prise, G. M. Tozer, G. R. Pettit and D. J. Chaplin, *Cancer Res.*, 1997, **57**, 1829–1834.
32 B. A. Salmon, H. W. Salmon and D. W. Siemann, *Eur. J. Cancer*, 2007, **43**, 1622–1629.
33 S. A. Hill, D. J. Chaplin, G. Lewis and G. M. Tozer, *Int. J. Cancer*, 2002, **102**, 70–74.
34 D. W. Siemann, D. J. Chaplin and P. A. Walicke, *Expert Opin. Invest. Drugs*, 2009, **18**, 189–197.
35 C. D. Ley, M. R. Horsman and P. E. Kristjansen, *Neoplasia*, 2007, **9**, 108–112.